Crossover from Classical to Fermi Liquid Behavior in Dense Plasmas

Jérôme Daligault

Phys. Rev. Lett. **119**, 045002 — Published 27 July 2017

DOI: 10.1103/PhysRevLett.119.045002

On the Crossover from Classical to Fermi Liquid Behavior in Dense Plasmas

Jérôme Daligault*
Los Alamos National Laboratory, Los Alamos, NM 87545, USA
(Dated: June 7, 2017)

We explore the crossover from classical plasma to quantum Fermi liquid behavior of electrons in dense plasmas. To this end, we analyze the evolution with density and temperature of the momentum lifetime of a test electron introduced in a dense electron gas. This allows us 1) to determine the boundaries of the crossover region in the temperature-density plane and to shed light on the evolution of scattering properties across it, 2) to quantify the role of the fermionic nature of electrons on electronic collisions across the crossover region, and 3) to explain how the concept of Coulomb logarithm emerges at high enough temperature but disappears at low enough temperature.

Dense plasmas are characterized by the coexistence of significant quantum, thermal and Coulomb coupling effects that push the classic descriptions of plasmas and condensed matter outside their limits of validity [1, 2]. In addition, by their intermediate nature, dense plasmas exhibit sharp transitions and smooth crossovers in their properties. A notable example is that of ionic properties. As the temperature is lowered and the density is increased from the hot and dilute plasma regime, the ions show evolution from a nearly collisionless gaseous regime, continuously through an increasingly correlated liquid-like regime, on to solidification [3]. Much is known about these regimes, mainly thanks to the ability to perform first-principle simulations of classical systems. Remarkably, a similar depiction of the properties of conduction electrons from the classical regime at high enough temperatures and low enough densities down to the fully Fermi degenerate regime at low temperatures and high densities, does not exist. An improved description of the crossover between the two regimes is desirable to advance our understanding and modeling capability of conditions that are routinely created in laboratory experiments [4–6], are traversed in inertial confinement fusion (ICF) experiments [7], and are common in stars and planets [8].

For simplicity, let us consider an infinite gas of electrons (number density n, charge $-e$, mass m) in a uniform neutralizing background and in thermal equilibrium at temperature T. The parameter commonly used to demarcate the passage from the classical to the Fermi degenerate regimes is the degenaracy parameter $\Theta = k_B T/E_F$, where $E_F = p_F^2/2m$ is the Fermi energy, $p_F = \hbar k_F$ is the Fermi momentum with $k_F = (3\pi^2 n)^{1/3}$. Traditional plasma physics applies at high enough T and low enough n such that $\Theta \gg 1$: electrons behave essentially like a classical, weakly coupled gas of point particles undergoing small-angle binary collisions; this regime is well described by the classical Fokker-Planck (FP) equation [9]. By contrast, at low enough T and high enough n such that $\Theta \ll 1$, electrons are in a state of complete Fermi degeneracy: this is the regime of Landau's theory of normal Fermi liquids that describes the gas of (possibly strongly interacting) electrons as a dilute collection of elementary excitations, or quasiparticles, whose dynamics is governed the quantum Boltzmann equation [10]. Striking differences exist between the dynamical properties of these two regimes. For instance, the transport coefficients show vastly different temperature dependence [11, 12]: the shear-viscosity coefficient $\eta \propto T^{5/2}$ for $\Theta \gg 1$ but is $\propto T^{-2}$ for $\Theta \ll 1$; similarly the thermal conductivity coefficient $\lambda \propto T^{5/2}$ for $\Theta \gg 1$ but is $\propto T^{-1}$ for $\Theta \ll 1$ [13]. The Pauli exclusion principle, which implies that, for $\Theta \ll 1$, only a small fraction $\propto \Theta$ of electrons around the Fermi surface are free to scatter with others, is responsible for these changes. Another usually disregarded but significant consequence is the dependence on the effective electron-electron interaction W. In the classical regime, η and λ are inversely proportional to the Coulomb logarithm $\ln\Lambda = \int_0^\infty dq q^3 \sigma(q)$, where $\sigma(q) \propto |W(q)|^2$ is the differential binary collision cross section and q the momentum transfer [14]. By contrast, in the Fermi liquid regime [12], η and λ are inversely proportional to $\int_0^{2k_F} dq \sigma(q)$, and this independently of the range of W. The disappearance of the Coulomb logarithm at small Θ suggests the breakdown of the grazing collisions approximation that underlies plasma theory. Incidentally, the quantum FP equation [15], which extends the classical equation by including the Pauli principle while keeping the small-angle collision approximation, predicts $\lambda \propto T^{-2}$ [16], in sharp disagreement with the above-mentioned T^{-1} scaling. Finally, whereas previous results ignore the effect of particle indistinguishability, it is known that exchange processes greatly reduce the scattering between parallel-spin electrons relative to that from antiparalllel-spin electrons at $\Theta \ll 1$ [17, 18], while being insignificant in the classical regime.

These results raise a number of open questions, including: What are the boundaries of the gap separating the classical plasma and Fermi liquid regimes? When does exchange become negligible? How does the Coulomb logarithm emerge from the quantum regime? When does the small-angle scattering approximation underlying plasma physics break down? These questions are important, not only from a basic standpoint to advance our fundamental understanding of dense plasmas, but also from a practical standpoint to guide the development of needed first-principle simulations that can access truly dynamical and

non-equilibrium regimes [19–21], while in current simulations electrons are not dynamical [22, 23]. An obvious approach to shed light on these questions is to calculate η and λ from the quantum Boltzmann equation across the gap. However a practical solution seems elusive due to the complexity of the collision operator. In this work, we instead consider a physical quantity, viz., the electron momentum lifetime, that is accessible to analytical treatment and numerical evaluation across the gap. We continue considering the electron gas model, which underlies numerous calculations in the field [1, 2, 24].

The momentum lifetime $\tau_{\mathbf{k}}$ is defined as the inverse collision rate of an extra electron with momentum $\mathbf{p}=\hbar\mathbf{k}$, which, at some time $t=0$, is suddenly introduced into an electron gas in thermal equilibrium and then scatters against its constituents [25]. We assume that the most relevant scattering process is the binary collision into a state of momentum $\hbar(\mathbf{k}+\mathbf{q})$ with an electron of initial momentum $\hbar\mathbf{k}'$, and that the colliding electrons interact through the static, exponentially screened Coulomb potential $W(q)=\frac{e^2}{\epsilon_0}\frac{1}{q^2+k_{sc}^2}\equiv\frac{e^2}{\epsilon_0}v(q)$ [32]. Here $k_{sc}=k_{DH}\sqrt{\mathcal{F}_{-1/2}/\mathcal{F}_{1/2}}$, where $\mathcal{F}_\nu(\mu/k_BT)$ is the Fermi function [26] and μ the chemical potential, is the inverse Thomas-Fermi screening length that varies from $2\sqrt{k_F/\pi a_B}$ at $T=0$ to the inverse Debye-Hückel length $k_{DH}=\sqrt{e^2n/\epsilon_0k_BT}$ at high T (see Fig. 1). By applying the Fermi golden rule to calculate the transition probability of a collision and summing over all allowed collisions in accordance to the Pauli principle and energy-momentum conservation [10, 18], we find $1/\tau_{\mathbf{k}}=1/\tau_{\mathbf{k}}^d-1/\tau_{\mathbf{k}}^{ex}$, where

$$\frac{1}{\tau_{\mathbf{k}}^d} = 2\frac{2\pi e^4}{\hbar\epsilon_0^2}\frac{1}{V^2}\sum_{\mathbf{k}',\mathbf{q}}|v(\mathbf{q})|^2 \times n_{\mathbf{k}'}(1-n_{\mathbf{k}+\mathbf{q}})(1-n_{\mathbf{k}'-\mathbf{q}})\delta(\epsilon_{\mathbf{k}+\mathbf{q}}+\epsilon_{\mathbf{k}'-\mathbf{q}}-\epsilon_{\mathbf{k}}-\epsilon_{\mathbf{k}'}) \quad (1)$$

$$\frac{1}{\tau_{\mathbf{k}}^{ex}} = \frac{2\pi e^4}{\hbar\epsilon_0^2}\frac{1}{V^2}\sum_{\mathbf{k}',\mathbf{q}}v(|-\mathbf{q}|)v(|\mathbf{q}+\mathbf{k}-\mathbf{k}'|) \times n_{\mathbf{k}'}(1-n_{\mathbf{k}+\mathbf{q}})(1-n_{\mathbf{k}'-\mathbf{q}})\delta(\epsilon_{\mathbf{k}+\mathbf{q}}+\epsilon_{\mathbf{k}'-\mathbf{q}}-\epsilon_{\mathbf{k}}-\epsilon_{\mathbf{k}'}), \quad (2)$$

with $\epsilon_{\mathbf{k}}=\hbar^2\mathbf{k}^2/2m$ and $n_{\mathbf{k}}=1/(1+e^{-(\mu-\epsilon_{\mathbf{k}})/k_BT})$. For convenience, we express $1/\tau_{\mathbf{k}}$ as a sum of a "direct" term $1/\tau_{\mathbf{k}}^d$, which treats electrons as distinguishable particles, and an "exchange" term $1/\tau_{\mathbf{k}}^{ex}$, which incorporates the effects of indistinguishability.

Direct term. We find it useful to express Eq.(1) as

$$\frac{1}{\tau_{\mathbf{k}}^d} = \omega_p k_{sc}^3\int_0^\infty dq\,|v(q)|^2\,G_{k/k_F,\Theta}\,(q/k_F)\,, \quad (3)$$

where $\omega_p=\sqrt{e^2n/\epsilon_0m}$ is the plasma frequency, and

$$G_{x,\Theta}(y)=\frac{9\pi}{16\sqrt{2}}\Theta^{\frac{5}{2}}\left(\frac{\mathcal{F}_{1/2}(\tilde{\mu}/\Theta)}{\mathcal{F}_{-1/2}(\tilde{\mu}/\Theta)}\right)^{\frac{3}{2}}y\int_{y/2-x}^{y/2+x}du \times\frac{1}{1-e^{\frac{2y}{\Theta}u}}\frac{1}{1+e^{-\frac{2y}{\Theta}u}e^{\frac{1}{\Theta}(\tilde{\mu}-x)}}\ln\frac{1+e^{\frac{1}{\Theta}\left[\tilde{\mu}-(u+y/2)^2\right]}}{1+e^{\frac{1}{\Theta}\left[\tilde{\mu}-(-u+y/2)^2\right]}}\,, \quad (4)$$

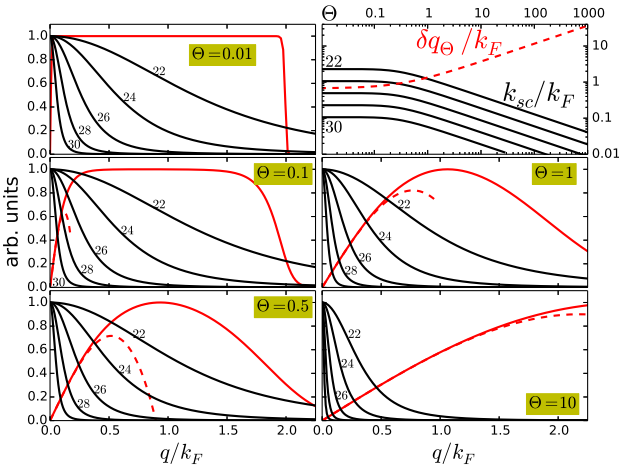

FIG. 1: (color online) Components of the integrand (3) for various Θ. The black lines show $|v(q)|^2$ for $n=10^m$ cm^{-3} with $m=22,\ 24,\ 26,\ 28,\ 30$. The red lines show $G_{k_\Theta/k_F,\Theta}(q/k_F)$ (full) rescaled to its maximum value (see Fig. 2) and the third-order Taylor expansion (dashed lines). Upper right panel: inverse screening length k_{sc}/k_F vs Θ for the same densities as above. The dashed line shows $\delta q(\Theta)/k_F$.

with $\tilde{\mu}(\Theta)=\mu/E_F$. Equation (3) gives the relaxation rate as the sum over $q=|\mathbf{q}|$ of the product of the differential cross section $\propto|v(q)|^2$, which selects the dominant scattering processes, times a universal factor G (dropping parameters), which measures the total number of collisions with momentum transfer $\hbar q$ that can occur in accordance with the Pauli principle and energy-momentum conservation. As illustrated in Fig. 1, by looking at how these two quantities vary and overlap with n and T, we can identify different physical regimes.

We first describe some features of G, giving special emphasis to its small-q behavior because of its central role in our later discussion. For definiteness, in Figs. 1 and 2, we set the initial momentum p to the relevant value $p_\Theta=\hbar k_\Theta=p_F\sqrt{1+\Theta/2}$, which varies from the Fermi momentum p_F at $\Theta\ll1$ to the thermal momentum $p_{th}=\sqrt{mk_BT}$ in the classical limit. With our choice of definitions, the analysis is simplified since G depends parametrically on Θ only [27]; thus, say by varying n at constant Θ, only $|v(q)|^2$ changes along with k_{sc}. As shown in Fig. 2, for $\Theta\ll1$, $G_{k_\Theta/k_F,\Theta}(q/k_F)$ is essentially constant between $q=0$ and $2k_F$ at a value $\propto T^2$, with a steep increase at $q=0$ (see inset) over a range $\delta q_\Theta/k_F\sim\sqrt{\Theta}$, and a steep decay at $q\simeq2k_F$, the maximum momentum transfer that scattering electrons at the Fermi surface can undergo. The change of behavior around δq_Θ results from a change in the phase-space restrictions imposed by the energy-momentum conservation and the Pauli principle, which constrain both $\mathbf{k}'$ and $\mathbf{k}'-\mathbf{q}$ before and after the collision with the extra electron to lie within a shell of thickness $\sim k_F\sqrt{\Theta}$ around the Fermi surface. If $\mathbf{k}'$ lies in the shell then $\mathbf{k}'$–$\mathbf{q}$ is automati-

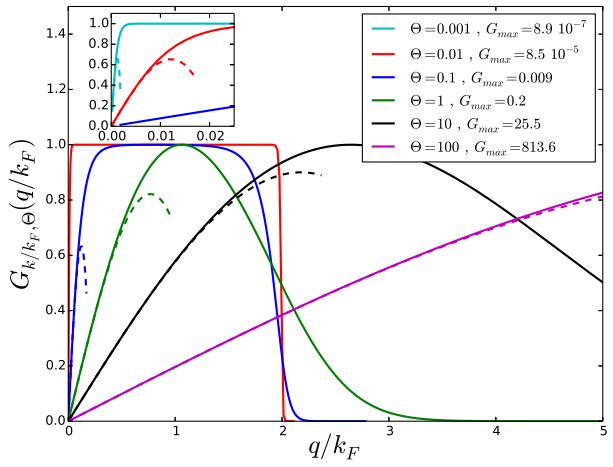

FIG. 2: (color online) Factor $G_{k_\Theta/k_F,\Theta}(q/k_F)$ (full lines) across degeneracy regimes; results for small Θ are magnified in the inset. For ease of comparison, all factors are rescaled by their maximum value G_{max} given in the legend. The dashed lines show the third-order Taylor expansion $G^{(3)}$.

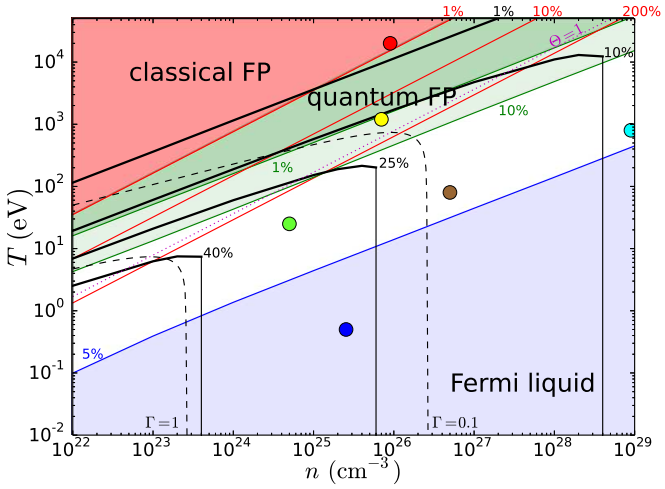

FIG. 3: Regimes of electronic collisions identified in this study displayed in a plot of temperature versus density. The lines and colors are defined in the text (page 4). For reference, the dots show the typical positions of ICF burning plasmas (red) and of the cores of astrophysical objects, including the Sun (yellow), white dwarfs before core solidification (cyan), brown dwarfs (brown), Jupiter (green), Earth (blue).

cally in the shell only if the momentum transfer is $q<\delta q_\Theta$, but it must be further constrained to lie in the shell if $q>\delta q_\Theta$. As Θ increases, the function G broadens along with the Fermi surface, and δq_Θ increases. We note that the expansion $G_{k_\Theta/k_F,\Theta}(q/k_F)\simeq G^{(3)}(\Theta,q)=a_1q+a_3q^3$ shown by the dashed lines in Figs. 1-2 is an excellent approximation for $q<\delta q_\Theta\equiv\sqrt{-a_1/3a_3}\simeq k_F\sqrt{0.45+4\Theta/3}$ [28], with δq_Θ set to the location of the maximum of $G^{(3)}$.

We then discuss the consequences on the momentum lifetime. In the literature on Fermi liquids (FL), the $\Theta\ll 1$ limit of Eq.(1) is usually given for k in the vicinity of the Fermi surface in the form

$$\frac{1}{\tau_{\mathbf{k}}^{\rm FL}}=\frac{2m^3e^4}{\epsilon_0^2\pi\hbar^7k}\frac{(\epsilon_{\mathbf{k}}-\mu)^2+(\pi k_BT)^2}{1+e^{-(\epsilon_{\mathbf{k}}-\mu)/k_BT}}\int_0^{2k_F}dq\;|v\,(q)|^2\,. \quad (5)$$

As said in the introduction, there is no Coulomb logarithm. The panel $\Theta=0.01$ in Fig. 1 gives a graphical explanation of this result: for all densities, $k_{sc}\gg\delta q_\Theta$, and the overlap between G and $|v|^2$ occurs predominantly in the constant part of G, which factorizes out of Eq.(3) to give Eq.(5). By contrast, in the non-degenerate limit $\Theta\gg 1$, $\mu/k_BT\ll -1$ and Eq.(3) simplifies to

$$\frac{1}{\tau_{\mathbf{k}}^{\rm cl}}=\frac{4\pi nme^4}{\hbar^3k}\int_0^\infty dq\,q\,|v(q)|^2\left[\mathrm{erf}\left(\frac{k+q}{\sqrt{\Theta}k_F}\right)+\mathrm{erf}\left(\frac{k-q}{\sqrt{\Theta}k_F}\right)\right]. \quad (6)$$

However, as illustrated in Fig. 1 for $\Theta=10$, $k_{sc}\ll\delta q_\Theta$ in this limit and $|v|^2$ overlaps entirely with the small-q expansion $G^{(3)}$ such that the direct term reduces to

$$\frac{1}{\tau_{\mathbf{k}}^{FP}}=A_1\int_0^{\delta q_\Theta}dqq|v(q)|^2+A_3\underbrace{\int_0^{\delta q_\Theta}dqq^3|v(q)|^2}_{\ln\Lambda}\,. \quad (7)$$

with $A_{1,3}(n,\Theta)=\omega_p(n)k_{sc}^3(n,\Theta)a_{1,3}(n,\Theta)$; we associate this expression to the FP description since it retains the small-angle collisions only. The traditional Coulomb logarithm $\ln\Lambda$ emerges from the third-order term a_3q^3 with the upper momentum transfer cutoff $\delta q_\Theta\simeq k_F\sqrt{4\Theta/3}=1.63/\lambda_{dB}$, where $\lambda_{dB}=\hbar/\sqrt{mk_BT}$ is the thermal de Broglie wavelength, which is consistent with the ad-hoc cutoff $\delta q_\Theta\simeq 1/\lambda_{dB}$ prescribed in the literature. One may find surprising that, unlike the usual transport coefficients of classical plasma theory, an extra term $\propto\int dqq|v(q)|^2$ also arises in Eq.(7). This is because in deriving the FP equation by expanding the Boltzmann collision operator in powers of $\mathbf{q}$ [11], the leading term is $\propto q^3$ since the lower orders, including q^1, cancel when the scattering-*in* and -*out* processes that change the distribution $f(\mathbf{p})$ of electrons are summed; by contrast, this cancellation does not occur here since the momentum lifetime includes only the processes that scatter a single test electron *out* its initial momentum $\mathbf{p}$. The results shown in Fig.(1) for $\Theta\leq 1$ illustrate that the FP behavior underlying classical plasma theory is not limited to non-degenerate plasmas but applies whenever k_{sc} and δq_Θ are such that $|v|^2$ and $G^{(3)}$ fully overlap. The temperature at which this first occurs depends on the density along with k_{sc}. For instance, at $\Theta=0.1$, $|v|^2$ and G still overlap predominantly in the range $q>\delta q_\Theta$ for all densities n shown except 10^{30} cm^{-3}; at $\Theta=1$ this is the case for $n<10^{26}$ cm^{-3} only; at $\Theta=10$, $|v|^2$ and $G^{(3)}$ fully overlap for all n.

By comparing numerically Eqs.(3)-(7) for $k=k_\Theta$, we identify the different regimes displayed in the T-n diagram shown in Fig. 3. The red area corresponds to conditions where $|(\tau_{\mathbf{k}}^{\rm cl}-\tau_{\mathbf{k}}^{d})/\tau_{\mathbf{k}}^{d}|\leq 0.01$ and is identified as

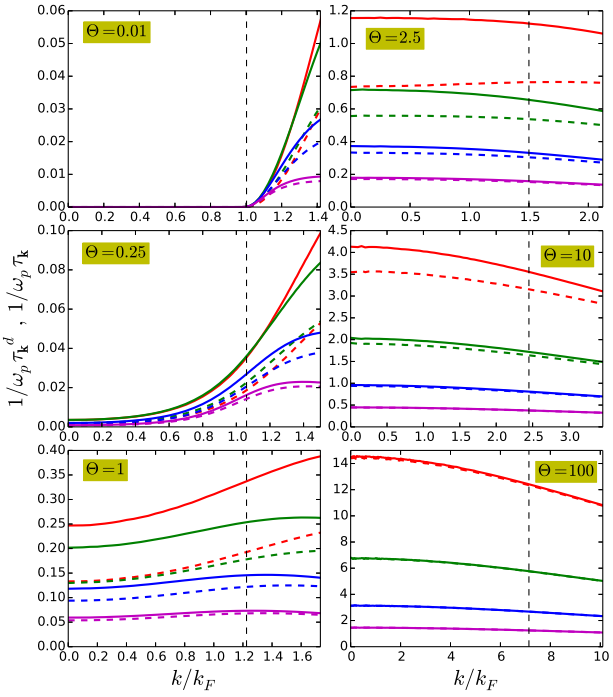

FIG. 4: (color online) $1/\tau_{\mathbf{k}}$ (dashed line) and $1/\tau_{\mathbf{k}}^d$ (full line) in units of $\omega_p(n)$ vs initial momentum k/k_F for a range of Θ and $n=10^m$ cm^{-3} with $m=22$ (red), 24 (green), 26 (blue), 28 (magenta). The vertical dashed lines indicate $k=k_\Theta$.

the "classical FP" region where classical plasma physics applies; for reference, since the previous criterion is reasonable but arbitrary, the red lines delimit regions above which $|(\tau_{\mathbf{k}}^{\rm cl}-\tau_{\mathbf{k}}^d)/\tau_{\mathbf{k}}^d|\leq 0.1$ and 2. The blue area corresponds to conditions where $|(\tau_{\mathbf{k}}^{\rm FL}-\tau_{\mathbf{k}}^d)/\tau_{\mathbf{k}}^d|\leq 0.05$, and is identified as the regime where the Fermi liquid theory applies. The crossover region that we set out to delineate lies between the red and blue areas. There, the green area corresponds to conditions where $|(\tau_{\mathbf{k}}^{\rm FP}-\tau_{\mathbf{k}}^d)/\tau_{\mathbf{k}}^d|\leq 0.01$ (dark green) and ≤ 0.1 (light green), and is identified as the "quantum FP" region where the small-angle collision approximation remains valid but degeneracy effects are non-negligible. In the white area, short-range collisions, degeneracy and thermal effects are non-negligible.

Other features of the crossover can be seen in Fig. 4, which shows $1/\tau_{\mathbf{k}}^d$ (full lines) for $0<k\leq\sqrt{2}k_\Theta$, $10^{22}\leq n\leq 10^{30}$ cm^{-3} and $0.01\leq\Theta\leq 100$. Briefly, at small Θ, we see the effect of the broadening of the Fermi surface: collision channels that are inhibited by the Pauli principle at $\Theta=0.1$ when $k<k_F$, are opened at $\Theta=0.25$. The non-degenerate limit (6) overlaps (not shown) with the exact expression (3) at $\Theta\geq 10$ only.

Exchange term. Figure 4 compares the total collision rate $1/\tau_{\mathbf{k}}$ (dashed lines) with the direct contribution $1/\tau_{\mathbf{k}}^d$ (full lines) for $10^{22}\leq n\leq 10^{28}$ cm^{-3} and $0.01\leq\Theta\leq 100$. Exchange processes always reduce the scattering rate and there are non-trivial variations with n and Θ. For instance, with $n=10^{28}$ cm^{-2} (purple lines), $R\equiv(1/\tau_{\mathbf{k}_\Theta}^{ex})/(1/\tau_{\mathbf{k}_\Theta}^d)$ is $\simeq 10\%$ for $0\leq\Theta\leq 0.5$, $=7\%$ at $\Theta=1$ and is $<0.5\%$ above $\Theta=10$. By contrast, at the lower densities, exchange remains non-negligible over a wider range of conditions; e.g., with $n=10^{22}$ cm^{-2} (red lines), $R\simeq 47\%$ for $\Theta\ll 1$ (note that Eqs(1-2) imply $R\leq 50\%$ for all n and T), $=45\%$ at $\Theta=1$ and is $<10\%$ only above $\Theta=10$. These variations are summarized in Fig. 3, where the black lines show the conditions at which $R=1\%$, 10%, 25% and 40%; these lines stop abruptly at a density (see vertical black lines) above which the criterion is never met. These variations reflect the type of collisions that predominate, which depends on the range of the electronic interactions, i.e. on the magnitude of k_{sc}. At small enough k_{sc}, collisions occur mostly between distant electrons and particle exchange is small. By contrast, at large enough k_{sc}, interactions are short-ranged and more prompt to particle exchange.

In summary, by calculating the evolution with density and temperature of the momentum lifetime of a test electron in a dense electron gas, we have explored the crossover from classical plasma to Fermi liquid behavior of electronic collisions not only in light of the degeneracy parameter Θ, which gives information of kinematic nature (i.e., related to the set of allowed collision processes), but also considering the range $1/k_{sc}$ of the effective electronic interactions, which gives information of kinetic nature by determining the dominant scattering processes. This allowed us to determine the boundaries of the crossover, to understand the emergence and extent of validity beyond the classical plasma regime of the notion of Coulomb logarithm, and to estimate the contribution of exchange processes. Our main findings are summarized in the T-n diagram of Fig. 3. Our calculations rely on several approximations that are suitable when the interactions between electrons represent a relatively small perturbation, i.e. when the ratio $\Gamma=\frac{e^2}{4\pi\epsilon_0 a}\frac{1}{\sqrt{(k_BT)^2+E_F^2}}$ ($a=(3/4\pi n)^{1/3}$) of the average potential energy per electron to the average kinetic energy is smaller than unity [30]. In Fig. 3, the dashed lines demarcate the regions above which $\Gamma\leq 1$ and 0.1, and show that our calculations are likely to be somewhat in error in the bottom left corner of the T-n diagram. The inclusion of Coulomb coupling effects is challenging but could be approached with sophisticated techniques like the GW method [31].

This work was performed under the auspices of the United States Department of Energy under Contract DE-AC52-06NA25396 and supported by LDRD Grant No. 20170490ER.

* Electronic address: daligaul@lanl.gov

[1] S. Ichimaru, *Statistical Plasma Physics, Vol. II: Condensed Plasmas*, Westview Press (2004).
[2] D. Kremp, M. Schlanges, and W.-D. Kraeft, *Quantum*

Statistics of Nonideal Plasmas (Springer, 2005).
[3] J. Daligault, *Phys. Rev. Lett.* **96**, 065003 (2006).
[4] P. Sperling, E.J. Gamboa, H.J. Lee, H.K. Chung, E. Galtier, Y. Omarbakiyeva, H. Reinholz, G. Röpke, U. Zastrau, J. Hastings, L.B. Fletcher, and S.H. Glenzer, *Phys. Rev. Lett.* **115**, 115001 (2015).
[5] A.B. Zylstra, J.A. Frenje, P.E. Grabowski, C.K. Li, G.W. Collins, P. Fitzsimmons, S. Glenzer, F. Graziani, S.B. Hansen, S.X. Hu, M. G. Johnson, P. Keiter, H. Reynolds, J.R. Rygg, F. H. Seguin, and R.D. Petrasso, *Phys. Rev. Lett.* **114**, 215002 (2015).
[6] B.I. Cho, T. Ogitsu, K. Engelhorn, A.A. Correa, Y. Ping, J.W. Lee, L.J. Bae, D. Prendergast, R.W. Falcone, P.A. Heimann, *Scientific Reports* **6**, 18843 (2016).
[7] A. C. Hayes, G. Jungman, A. E. Schulz, M. Boswell, M. M. Fowler, G. Grim, A. Klein, R. S. Rundberg, J. B. Wilhelmy, D. Wilson, C. Cerjan, D. Schneider, S. M. Sepke, A. Tonchev and C. Yeamans, *Phys. Plasmas* **22**, 082703 (2015).
[8] H.M. Van Horn, Science *252*, 384 (1991).
[9] M.N. Rosenbluth, W.M. MacDonald, and D.L. Judd, *Phys. Rev.* **107**, 1 (1957).
[10] D. Pines and P. Nozières *The Theory of Quantum Liquids, Vol.1* (Benjamin Inc., New York, N. Y., 1966).
[11] L.P. Landau, E.M. Lifshitz and L.P. Pitaevskii, *Physical Kinetics, Vol. 10* (Elsevier Ltd, 1981).
[12] A. A. Abrikosov and I. M. Khalatnikov, *Rep. Prog. Phys.* **22**, 329 (1959).
[13] The complete expressions are [11, 12]

$$\eta = \begin{cases} \dfrac{5\sqrt{\pi m}}{8q^4}\dfrac{(k_BT)^{5/2}}{\ln\Lambda} & , \quad \Theta \ll 1 \\ \dfrac{16}{45}\dfrac{\hbar^3 p_F^5}{(4\pi m^2 q^2)^2}\dfrac{(k_BT)^{-2}}{\left\langle W(k)\sin^4(\theta/2)\sin^2(\phi)/\cos(\theta/2)\right\rangle} & , \quad \Theta \gg 1 \end{cases}$$

$$\kappa = \begin{cases} \dfrac{75k_B}{32\sqrt{m\pi}q^4}\dfrac{(k_BT)^{-5/2}}{\ln\Lambda} & , \quad \Theta \ll 1 \\ \dfrac{4\pi^2}{3}\dfrac{k_B(\hbar p_F)^3}{m^4(4\pi q^2)^2}\dfrac{(k_BT)^{-1}}{\left\langle W(k)\sin^2(\theta/2)/\cos(\theta/2)\right\rangle} & , \quad \Theta \gg 1 \end{cases}$$

with $k = 2k_F\sin(\theta/2)\sin(\phi/2)$ and $\langle . \rangle = \frac{1}{4\pi}\int_{4\pi} d\Omega$ an average over solid angles Ω.
[14] With the Coulomb interaction $W(q) \propto q^{-2}$, one recovers the standard expression $\ln\Lambda = \int dq/q$.
[15] J. Daligault, *Phys. Plasmas* **23**, 032706 (2016).
[16] M. Lampe, *Phys. Rev.* **170**, 306 (1968); **174**, 276 (1968).
[17] D.R. Penn, *Phys. Rev. B* **22**, 2677 (1980).
[18] Z. Qian and G. Vignale, *Phys. Rev. B* **71**, 075112 (2005).
[19] Z. Chen, B. Holst, S. E. Kirkwood, V. Sametoglu, M. Reid, Y. Y. Tsui, V. Recoules, and A. Ng, *Phys. Rev. Lett.* **110**, 135001 (2013).
[20] J. Clérouin, G. Robert, P. Arnault, C.Ticknor, J.D. Kress, and L.A. Collins *Phys. Rev. E*, **91** 011101(R) (2015).
[21] A.D. Baczewski, L. Shulenburger, M.P. Desjarlais, S.B. Hansen, and R.J. Magyar, Phys. Rev. Lett. **116**, 115004 (2016).
[22] *Frontiers and Challenges in Warm Dense Matter*, Series: Lecture Notes in Computational Science and Engineering, 96, edited by F. Graziani, M.P. Desjarlais, R. Redmer, and S.B. Trickey (Springer 2014).
[23] T. Sjsotrom and J. Daligault, *Phys. Rev. Lett.* **113**, 155006 (2014) and references therein.
[24] T. Dornheim, S. Groth, T. Sjostrom, F.D. Malone, W.M.C. Foulkes, and M. Bonitz, *Phys. Rev. Lett.* **117**, 156403 (2016).
[25] For the densities considered, relativistic effects are negligible since $p_F/mc < 1$.
[26] $\mathcal{F}_\nu(x) = \frac{1}{\Gamma(\nu+1)}\int_0^\infty dy \frac{y^\nu}{e^{y-x}+1}$.
[27] From $n = 2\mathcal{F}_{1/2}(\mu/k_BT)/(2\pi\lambda_{dB}^2)^{3/2}$, we find $na^3 = \frac{3}{4\pi} = \frac{9}{32\sqrt{\pi}}\Theta^{3/2}\mathcal{F}_{1/2}(\tilde{\mu}/\Theta)$, which shows that $\tilde{\mu}$ and G are functions of Θ only.
[28] The expansion demands a lengthy calculation; $a_{1,3}$ will be given elsewhere; we only give the simple fit $\delta q_\Theta \simeq k_F\sqrt{0.45+4\Theta/3}$, which is accurate for Θ values where the FP model introduced below is valid.
[29] W.H. Press, S. A. Teukolsky, W. T. Vetterling, and B. P. Flannery, *Numerical Recipes* (3rd Edition, Cambridge University Press, 2007).
[30] This definition conveniently varies from the classical value $e^2/4\pi\epsilon_0 a k_B T$ for $\Theta \gg 1$ and $e^2/4\pi\epsilon_0 a E_F$ for $\Theta \ll 1$.
[31] L. X. Benedict, C. D. Spataru and S. G. Louie, *Phys. Rev. B* **66**, 085116 (2002).
[32] The calculations could be extended to include dynamical screening effects. This is not necessary here since we limit ourselves to momenta $p \sim p_\Theta$ that do not have enough energy to excite a plasmon.